2025,Volume 2 , Issue 8 , PSIJK (16-27)

Pure Sciences International Journal of Kerbala

Sensing Aspects of Hybrid SERS Sensors HO-Si Pillars and SiQDs Integrated with Gold Nanoparticles: A Comparative Study

Hind Kh. Abbas [a*], Ali F. Al-Rawaf [a], Alwan M. Alwan [b]

[a] *Department of Physics, College of Education for Pure Science, University of Kerbela, Karbala-Iraq*
[b] *School of Applied Science, University of Technology, Baghdad-Iraq*

P A P E R I N F O

Received: 07.10.2025
Accepted: 27.10.2025
Published: 31.12.2025

Keywords:
SERS sensor, silicon nanostructures, laser induced etching

A b s t r a c t

Two types of hybrid SERS sensors, have been synthesized through integrated Au nanoparticles on horizontal oriented (HO)-Si pillars and Silicon quantum dots (SiQDs) nanostructures substrates . Aggressive Laser-induced etching process ; at high laser intensity of 450, and 550 mW/cm2 and 405 nm wavelength, was used to create the HO-Si pillars and SiQDs substrates respectively . The hybrid SERS sensors have been synthesized with simple, easy – to- work and very low cost dipping technique of HO-Si pillars and SiQDs based-substrates in HAuCl4 solution. The growth mechanism of Au nanoparticles has shown clear depending on the morphology of the based- substrate. In the case of HO-Si pillars, the creation of Au nanoparticles essentially happened at the surface of Si substrate rather than the surface boundaries of HO-Si pillars, whereas with using SiQDs substrate, the deposition of Au nanoparticles mostly occurred around the SiQDs substrate. The better performance of hybrid SERS sensor of higher development factor, with minimum LOD and outstanding reproducibility has been attained for SiQDs sensor rather than that of HO-Si pillars sensor of about (7.46 × 108) , (9*10 -14 M) and (4%), respectively.

DOI: 10.53851/psijk.v2.i8.16-27

1. INTRODUCTION

Silicon nanostructures and their different types (vertical and horizontal silicon pillars , silicon quantum dots and nanowires) are among the basic elements of high importance in the manufactures of different types of hybrid sensors, because of its great specific surface area and extraordinary propensity to react with various kinds of chemical elements (Canham, L. T. 1990, Alwan, A. M. 2008). The plasmonics characteristics of the Au nanoparticles , like the resonance frequency of surface Plasmon and enormous Raman scattering cross section of distinct Au nanoparticles create them as a correct candidates for chemical molecular category through using the SERS process in hybrid structures sensors (Wali, L. A. 2023, Naseef, I. A. 2019), so the creation of hybrid SERS sensors with Au nanostructures has been an vigorous research capacity owing to their exceptional optical properties, which intensely count on dimensions, form and composition (Cheng, X. Y. 2015, Rashid, R. B. 2022, Chalhoub, A. E. 2011, Alwan, M. A. 2007, Ershov, I. A. 2020). Silicon nanostructures were synthesized by a different wet etching process , like laser ablation in liquid , metal boosted chemical etching pathway , laser pyrolysis and Laser-induced etching process (Jubair, D. S. 2021). The latter preparation method is characterized by its simplicity , low cost and the ability to control the specifications of the resulting nanostructures layer by

*Corresponding Author Institutional Email:
hind.khab@uokerbala.edu.iq (Hind Khudheyer Abbas)

controlling the intensity of the laser beam in addition to the irradiation period of the laser beam (Dheyab, A. B. 2019, Kumar, V. 2013, Alwan, A. M. 2018, He, Y. 2019, Ali, W. H. 2020, Zhang, Y. 2005). An aggressive Si etching path with assisting laser beam is a tedious process to dissolve Si happen in high laser intensity at temperatures above ambient temperatures. In this etching path, two phenomenon happen, the first one is to remove the Si nanoparticles layer formed by surface etched to form colloidal nanostructures. While , the second process is that increase the temperature to an active degree leads to a decrease in the surface tension of etching solution (Alwan, A. M. 2017). This results in the removed Si nanostructures layer reverting back to the precipitate on the etched zone (Liu, L. R. 2019). In basic idea , the route of aggressive engraving is very close for laser pyrolysis pathway in terms of using a pulsed or continuous laser beam, as a heating source, to precipitate many elements (Wail, H. A. 2018). High laser intensity and focusing ability of the laser beam is embodied in the efficient tuning of variable dimensions of nanostructures (Liu, Y. N. 2018). This technology is based on high temperature substrate, where heat buildup helps the nanostructures to be deposited (Alwan, A. M. 2018). The use of the enhanced etching technique with a high-intensity laser beam accompanied by a high temperature in the production of unique nanostructures such as SiQDs and Ho si pillar as a function of the laser beam intensity and temperature was studied extensively (Hamoudi, W. K. 2020). And they reached distinguished results, where there was a fundamental change in the morphology and structural properties of the resulting nanostructures with increasing the intensity of the laser beam. For Giorgis et al , they fabricate and explore the characteristics of various types of hybrid structures sensors through integrating different noble metals, like Pt, Ag, and Au on vertically aligned Si nano-wires (VO-Si NWs) (Giorgis, F. 2008). Naseef et al, they synthesized (VO-Si NWs) via metal-boosted chemical etching pathway through employing silver nanoparticles as a catalyst and the VO-Si NWs layer was used as room temperature gas sensors (Naseef, I. A. 2017). In the current study , the role of the Silicon nanostructures type (HO-Si pillars and SiQDs) which is on the formation and performance of HO-Si pillars and SiQDs / Au nanoparticle hybrid SERS sensors have been studied based on the plasmonics features of the Au nanoparticles which is synthesized via gold ions reduction process. The main objective of this study is develop an efficient hybrid SERS sensor with higher development factor, with minimum LOD and reproducibility.

2 .EXPERIMENTAL WORK

2.1 Preparation of Si HO-Si pillars and SiQDs nanostructures substrates .

To obtain HO-Si pillars and SiQDs nanostructures substrates, a resistivity (100 Ω.cm), mono-crystalline (100), n-type Si wafer, was employed as substrate for an aggressive Laser-induced etching process. The etching condition involving a solution consist of a mixtutre of HF and high purity ethanol with a mixing ratio of (1 HF 48% :4 C2H5OH 99.99%), 19 min etching time, 55mA/cm2 etching current density and the temperatures varies with the laser illumination intensity . The aggressive Laser-induced etching process, involving using high laser intensity of 450, and 550 mW/cm2 of 405 nm wavelength, to create the HO-Si pillars and SiQDs nanostructures substrates respectively.

A schematic illustration of the etching process is shown in Fig. 1. The temperature at the irradiated area as a result of laser-substrate interaction process is measured using digital laser probe thermometer type (Lutron250). Later the etching process, the HO-Si pillars and SiQDs substrates was stored in high purity 99.9% methanol in order to prevent the occurrence of SiO2 layer over the synthesized nanostructures.

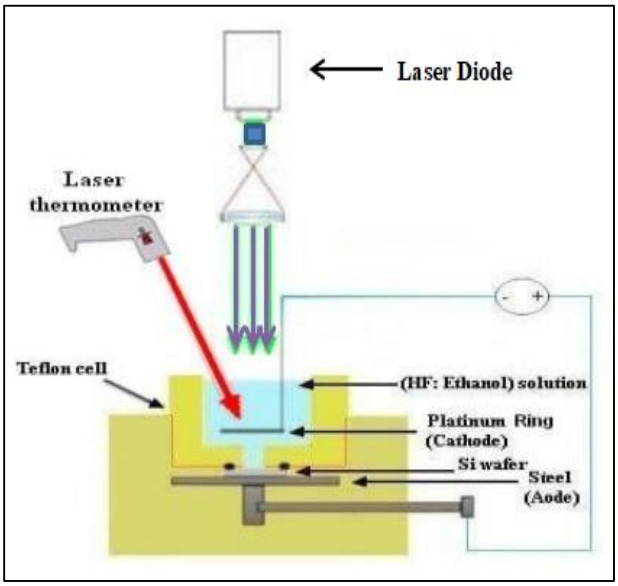

Figure 1. Schematic illustration of aggressive Laser-induced etching process

2.2 Production of hybrid SERS sensors.

In order to synthesis of HO-Si pillars and SiQDs / Au nanoparticle hybrid SERS sensors , a dilute solution of $6x10^{-3}$ M of high purity 99.9% salt was used by dissolving a specific weight of this salt in deionized distilled water. The HO-Si pillars and SiQDs based- nanostructures substrates were immersed for 2 minutes at room temperature, in the prepared $HAuCl_4$ solution which contains the Au-ions. The formation of Au nanoparticle above the HO-Si pillars and SiQDs nanostructures and hence the formation of hybrid SERS sensors was carried out through Au-ion reduction by Si–H dangling bonds on the surfaces and boundaries of Si nanostructures as presented in the formula (1) (Pohl, U. W. 2018).

Depending on the morphological nature of the Si nanostructures layer, the density of Si–H dangling bonds varied

$$Au^{+3} + 3e^{-} \rightarrow Au_{Nanoparticles} \quad (1)$$

The schematic representation of dipping technique of HO-Si pillars and SiQDs based-layers in HAuCl4 solution to synthesis the hybrid SERS sensors is illustrated in Figure 2.

The R6G solution with different concentrations ranging from 1.0×10^{-6} to1.0×10^{-12} M were used to identify the hybrid SERS sensors. While HO-Si pillars and SiQDs based- nanostructures substrate were tested at higher concentrations of about 1.0×10^{-4} .Every SERS sensor and based- nanostructures substrate were immersed into 25 mL of R6G solution for 5min to guarantee R6G adsorption on the nanostructures surface.

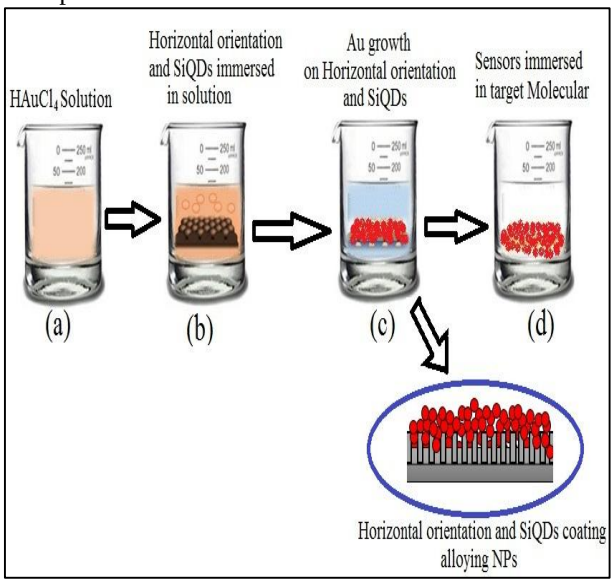

Figure 2. Schematic representation of formation **Au** nanoparticles by dipping technique.

2.3 Characteristic Techniques

The Structural, morphological characteristic of HO-Si pillars and SiQDs based-substrate and hybrid SERS sensors with plasmonics Au nanoparticles layer were analyzed using FE–SEM (FE–SEM; VEGA/TESCAN, XRD (XRD – 6000, Shemadzu power diffraction system with CuKα X–ray tube (λ=0.154056 nm),. Room temperature photoluminescence PL spectra were measured by system type (PL; Cary Eclipse FL 0912M014) with He Cd excitation laser wavelength of 320 nm. The Raman spectra of the of R6G dye deposited on HO-Si pillars and SiQDs based-substrate and hybrid SERS sensors were inspected with the dispersive Raman microscope (Senterra 2009, Bruker, Germany) with 785 nm and50 mW laser wavelength and power respectively . For each spectrum, the integration time was set as 10 s. To calculate the size distribution , surface density of SiQDs ,HO-Si pillars , and Au nanoparticles ,the dimensions of hotspot regions among Au nanoparticles from the FE-SEM a image special Image J software was used .

1. RESULTS AND DISCUSSIONS

3.1 Morphological aspects of HO-Si pillars and SiQDs nanostructures substrate and hybrid SERS sensors.

Figure 3a,d, display the FE-SEM images of HO-Si pillars and SiQDs based- nanostructures substrate .The morphological aspects of these type of nanostructures signifies a very significant factor in the growth and development of Au nanoparticles , where the nucleation sites (Si–Hx) dangling bonds are changed according to the morphology of the nanostructures substrate. The dangling bonds in the porous silicon layer play a fundamental role in the morphological properties of the nanomaterial layer deposited on it. The higher the density of the dangling bonds, the higher the reduction rate of the nanomaterial ions, and thus the growth rate of the nanoparticles increases and their size decreases (Wang, X. 2022). These different types of nanostructures substrate have been synthesized via various laser intensity. According to analysis of FE-SEM images, there were two specific forms of nanostructures morphologies:

1. The synthesis of non-connected HO-Si pillars nanostructures with a uniform cylindrical shape at different sizes deposited in random way over the etched zone ; Figure 3a. The cross-section form of the HO-Si pillars were almost spherical with diameters ranging from 30 to 70 nm, and lengths of the cylinder ranging from 80 to 350 nm. The surface density of this nanostructures was around $9x10^{8}$ Pillars.cm^{-2}. This

specific forms of nanostructures was synthesized on the Silicon surface at 450 mW/cm^2 laser intensity.

2. The synthesis of non-connected SiQDs nanostructures with orderly regular shape (approximately spherical form) and noteworthy low spam sizes; fig 3b. The surface density of SiQDs was around 3*10^{10} QDs.cm^{-2} with sizes ranging from 38 to 85 nm, and a highest distributed sizes located at 68 nm. This type of nanostructures was synthesized on the Silicon surface at 550 mW/cm^2 laser intensity.

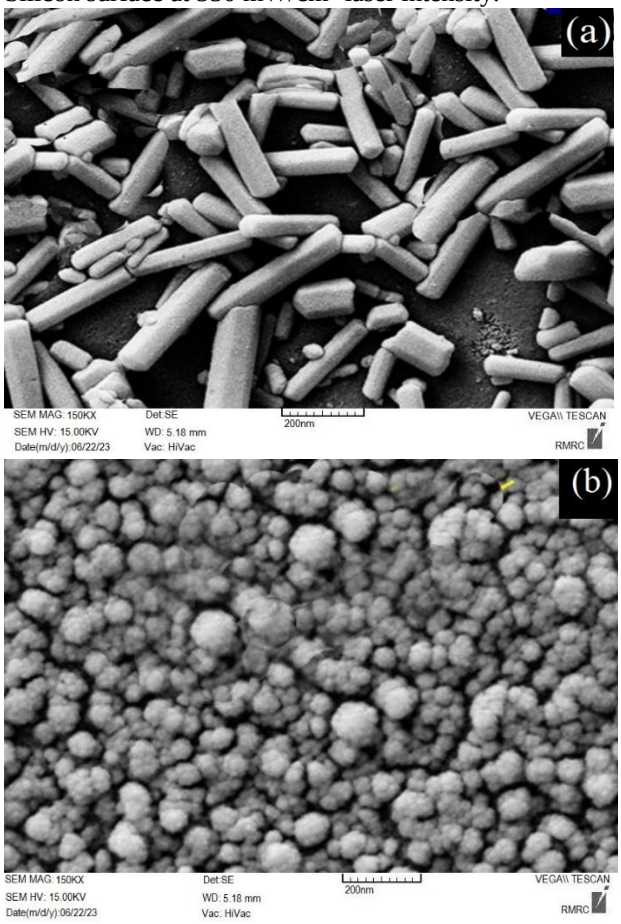

Figure 3. FE-SEM images of a) HO-Si pillars and b) SiQDs based- nanostructures substrate.

The Morphological aspects of the created Si nanostructures substrate can be understood as a distinctive imprint of the specification laser beam used in the aggressive etching process; particularly the intensity of the laser beam $\mathbf{p_{in_p}}$. An increase of the irradiating laser intensity can alter the photocurrent I_{photo} and therefore; the Si dissolution manner. The aggressive etching way be determined by the value of I_{photo} which is known via formula (2) (Alwan, A. M. 2014).

$$I_{Photo} = (1 - R_{Si\ Nano})P_{inp} \times \eta \times q/h_{\upsilon_o} \quad (2)$$

Where $R_{Si\ Nano}$ and η signifies the reflectivity and quantum efficiency of the Si nanostructures substrate respectively. While, $\mathbf{p_{in_p}}$ and υ_o presents the etching laser power and frequency of incident beam. Whereas h and q refer to Planck's constant and q is the electron charge respectively. The formation of HO-Si pillars and SiQDs nanostructures definitely be contingent on the Si dissolution manner as a result of the existence of positive holes at the Si nanostructures. These h^+ are formed both optically through the absorption of the laser photons and thermally through growing the temperature of the Si wafer in the course of the etching process (Abed, H. R. 2019). Consistent with K. Cheah hypothesis (Ko, F. H. 2015), the etching rate in the course of the aggressive Laser-induced etching path happens in 3-D directions x, y, and z. x and y signify the plane etching rate at the superficial upper layer, whereas z signifies the perpendicular etching rate on the wafer. The thermally-induced etching happens in 3-D directions but more rapidly in the illuminated zone, consequently, this etching will remove the synthesized Si nanostructures layer at the etched zone. The thermally and optically induced etching rates are ruled by means of the diffusion rate and the drift velocity of h+ to the illuminated zone (Wali, L. A. 2020). A particular quantity of the incident laser power will convert into heat P_{hea} inside the Si nanostructures and will lead to increase the temperature ΔT_r as exposed in formula (3) (Wali, L. A. 2020).:

$$\Delta T_r = P_{hea}/mcv \quad (3)$$

Where; $\Delta \boldsymbol{T}_r$ is the temperature rise and P_{hea} presents the portion of incident input laser power which is concerts to heat in substrate in the course of the etching path. The P_{hea} is connected to η via the following formula (4).

$$P_{hea} = (1 - \eta) \times (\text{laser power}) \quad (4)$$

Therefore, increasing the power of the laser beam falling on the substrate during etching will lead to an accelerated rise in temperatures in the substrate and in the liquid layer adjacent to it. Practically, increasing the power from 450 to 550 mW led to an increase in the temperature from 44 to 68 C^o. This sharp rise in the temperature of the substrate and the zone adjacent to it is mainly caused by the small wavelength of the laser beam used , which is 405 nm , as the smaller wavelength , the shorter the absorption depth (Alwan, A. M. 2011). So, the depth of absorption of the laser beam will be superficial and does not occur deep in the substrate, and therefore the temperature rise will be high

within the etching area, especially the surface layer. One of the results of this high temperature, in addition to the low value of thermal conductivity of the silicon nanostructures, is the acceleration of the removal of the silicon nanostructures resulting from etching and the formation of a colloidal solution in the etching space (Chang, C. C. 2012, Jabbar, A. A. 2020, Hou, X. 2011, Khalaf, A. A. 2021).

The thermal conductivity of silicon nanostructures is a function of the sizes of nanostructures, as the size was decreased, the thermal conductivity will decrease. For silicon nanostructures with a size of 60 to 200 nm, the value of thermal conductivity is round 0.74 W/m/K (Alwan, A. M. 2015), while the thermal conductivity of silicon is 160 W/m/K (Sychugov, I. 2005). This, in turn, will increase the possibility of removing nanostructures due to the increased thermal etching rate.

This, in turn, will also increase the possibility of fragmentation of silicon nanostructures of HO-Si pillars and SiQDs . Therefore, the aggressive etching process at high laser intensities and high temperature will modify the morphological aspects of nanostructures. According to the heating effect in the laser – substrate interaction and the superficial zone of solution (wealthy with colloidal suspension nanostructures), the proposed mechanism of HO-Si pillars and SiQDs structures growth overhead the etched substrate happened via the deposition of colloidal nanostructures in a path very near to laser pyrolysis method (Sulaiman, D. 2022, Xu, S. H. 2003, Alwan, A. M. 2020, Xu, S. H. 2003).

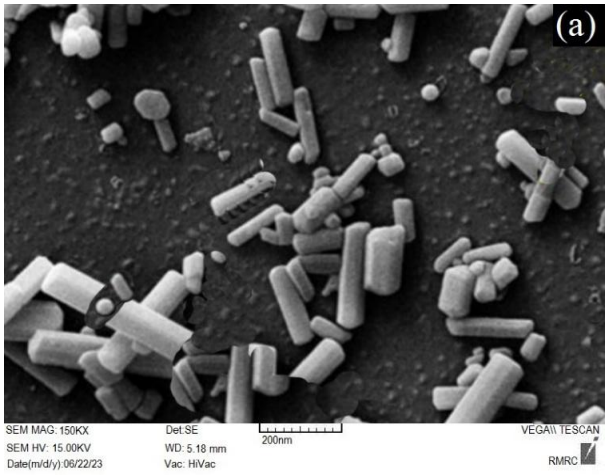

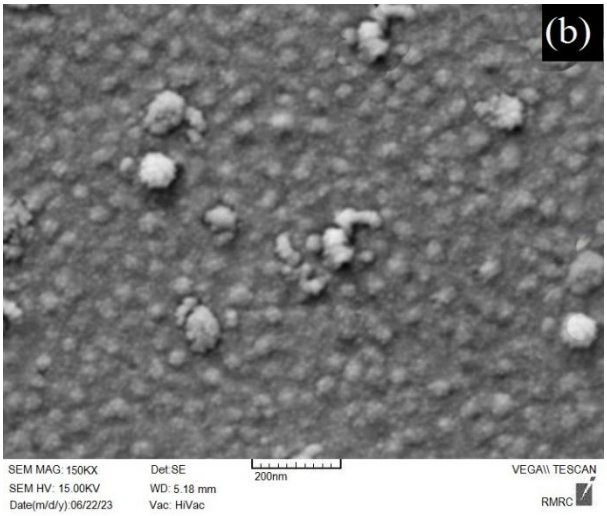

Figure 4. FE-SEM images of a) HO-Si pillars and b) SiQDs based- nanostructures substrates.

Fig 4a,b, shows the FE-SEM images of HO-Si pillars and SiQDs nanostructures later integrating the Au nanoparticles (hybrid SERS sensors). Since the amount of nucleation sites ($Si–H_x$) dangling bonds which is changed reliant on the morphology of the synthesized Si nanostructures layer. The Au nanoparticle were deposited in based on the Weber-Vomer mechanism, in which the formation of Au nanoparticle essentially happened at the lower etched Silicon layer owing to the immediate development of Au nanoparticle through Au ion reduction by dangling bonds on the faces of Si nanostructures . This deposition manner of nanoparticles have a large tendency to bury the lower etched silicon region and leads to remove some of HO-Si pillars and SiQDs nanostructures from the created layer.

The EDX spectra of Au nanoparticle deposited on HO-Si pillars and SiQDs nanostructures are exposed in fig 5a, b where the development of Au nanoparticle and the presence of Si materials is revealed. From this figure, it is obvious that the amount of Au nanoparticles differs with the type of nanostructures of layer. The amount of Au nanoparticle in the SiQDs substrate was greater than that of the HO-Si pillars substrate; as a result of the higher gold ion reduction centers in the SiQDs.

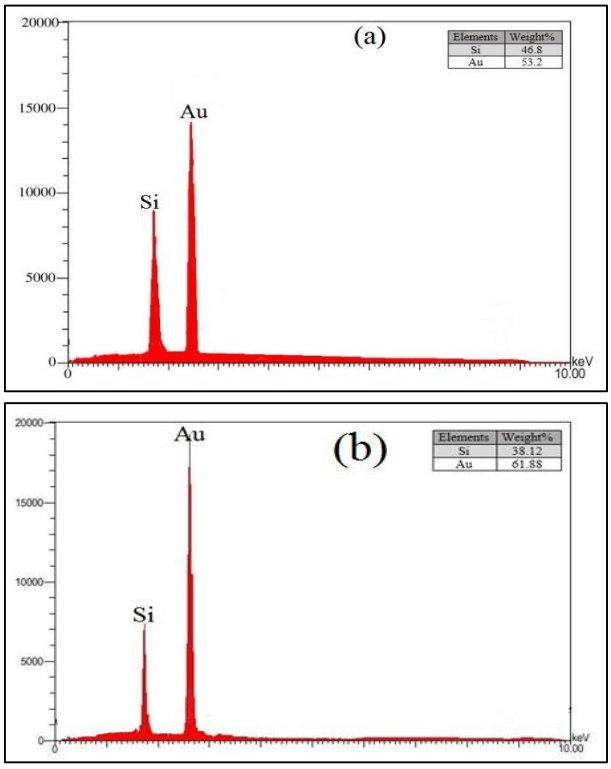

Figure 5. The EDX pattern of hybrid SERS sensors a) HO-Si pillars and b) SiQDs.

The XRD patterns of the Au nanoparticle/ HO-Si pillars and Au nanoparticle / SiQDs, hybrid SERS sensors correspondingly, are demonstrated in Fig. 6(a,b) ,which displays that for both of HO-Si pillars and SiQDs hybrid SERS sensors just a one specific diffraction peak seemed at 2θ about of 32.9° which is allocated to the (100) plane of crystalline Si consistent with the standards (JCPDS). Also , this Figure , shows two particular peaks located at 2θ around of 38.3° and 44.38° for the Au nanoparticle / HO-Si pillars and at 2θ about of 38.38° and 44.37° for the Au nanoparticle / SiQDs, hybrid which are allocated to the (111) and (200) crystal planes of Au, correspondingly. These diffraction peaks are in good match to pure Au element with face centered cubic symmetry (FCC). These diffraction peaks is clearly widened as related with bulk Au, signifying the creation of Au nanoparticle. From this diffraction pattern, it is obvious that the Au deposition process indications to the reducing in the diffraction peaks of the (100) plane of Si, this is recognized to the covering of the nanostructures surfaces by the Au nanoparticle. The sizes of the Au nanoparticle (D) are computed via Scherrer's equation (5) (Rashid, R. B. 2022) as follows:

$$D = \frac{0.9\lambda}{\beta \cos\theta} \quad (5)$$

Where, θ, β are diffraction angle (degree) and full width at half maximum (radians) respectively , while λ presents the wavelength in nm of employed radiation .

The Specific surface area of metallic nanoparticles (S) in hybrid structures is a very important parameter that indicates the efficiency of the hybrid SERS sensor. The efficiency of the hybrid sensor increases with the increase in its surface area . The (S) of the sensor is calculated depending on the size (D) and the density ρ_{Au} of of metal nanoparticle with the following relation (6) (Rashid, R. B. 2022).

$$S = \frac{6000}{\rho D} \quad (6)$$

For the (111) crystal plane, the value of D and S of Au nanoparticle are 7.26 nm and 35.41 m^2 /g, correspondingly, for Au nanoparticle / HO-Si pillars and 4.3 nm and 51.1 m^2 /g for Au nanoparticle / SiQDs, hybrid SERS sensor , correspondingly. As the FE–SEM images specify the agglomerated Au nanoparticle sizes, of the hybrid SERS sensor which were assessed from the XRD pattern are lower than that of attained from the FE–SEM images. The greater nanoparticles is strongly related with the propensity of the Au nanoparticle to conglomerate as a result of their excessive surface energy and surface tension among the ultrafine nanoparticles (Rashid, R. B. 2022).

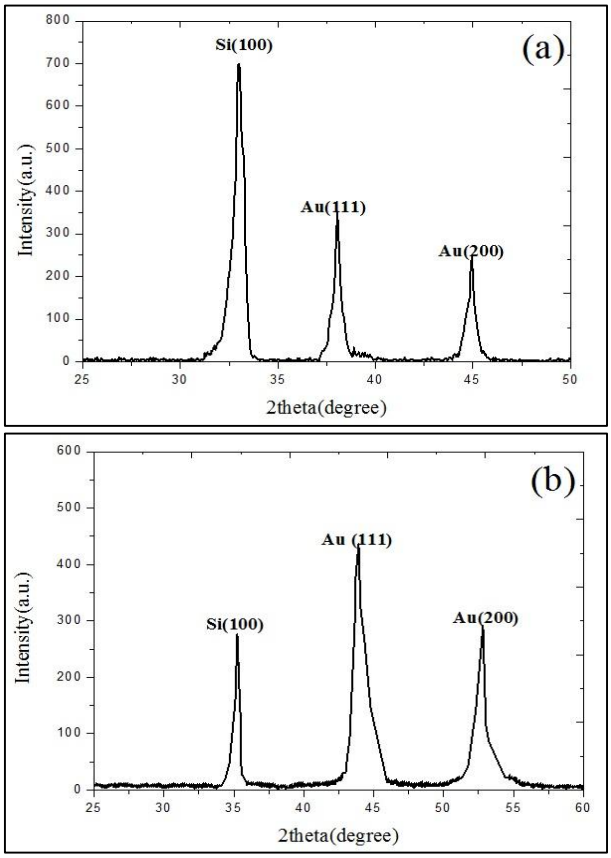

Figure 6. The XRD patterns of hybrid SERS sensors a) HO-Si pillars and b) SiQDs.

The photoluminescence spectra (PL) of HO-Si pillars and SiQDs based- nanostructures substrate and hybrid SERS sensors are presented in fig 7 a,b. The emission PL patterns be influenced by the morphology of the based- nanostructures substrate, the amount of Si nanostructures species , the amount of nucleation sites ($Si–H_x$) dangling bonds and the morphology of the Au nanoparticle on the hybrid SERS layer. The wavelengths and intensity of the emission PL, in addition to energy gap, and the enhancement factor of PL intensity were tabulated in table 1. As of this table, earlier integrating Au nanoparticle, shortest PL emission wavelength, i.e greater energy gap (Eg) was attained for SiQDs nanostructures, whereas longest PL emission wavelength, i.e lesser energy gap was recognized with HO-Si pillars nanostructures. Also; for SiQDs hybrid SERS sensor, exposed a higher peak intensity compared their comparative based- nanostructures substrate. This manners took place via the Si nanostructures involved with Au nanoparticle; due to the cancelling the effects of the (Si–Hx) dangling bonds ,which essentially act as nonradiative recombination sites which works to reduce the emission intensity resulting from the Si nanostructures . Furthermore, the FWHM of the PL emission from Si nanostructures was reduced with blue shifting in PL emission wavelength later integrating the Au nanoparticles. The hybrid SERS sensor of SiQDs, has a much higher intensity compared with the hybrid SERS sensor HO-Si pillars due to higher surface density of SiQDs in sensing area. The enhancement factor (e.f) in the intensity of PL emission after the integrating of Au nanoparticle is a strong evidence to investigate the activity of the hybrid SERS sensors. As the enhancement factor increases, the efficiency of the sensor increases. The concentration of gold ions is an important factor in determining the morphology of the gold nanoparticle layer deposited on the porous silicon surface. Increasing the concentration of gold ions leads to an increase in the surface density of gold nanoparticles, which in turn enhances the SERS-based sensing process. This in turn leads to an increase in the Raman signal intensity, and consequently, an increase in the Raman enhancement factor (E.f.). The value of e.f was around 2.1, and 0.45 for hybrid SERS sensor of Au nanoparticle / SiQDs and Au nanoparticle / HO-Si pillars, respectively. The increasing PL intensity is mainly depended on the amount of nanocrystallites' luminescence in the synthesized substrate owing to the rise of electron-hole recombination rate substrate [10]. The reliance of energy gap (Eg) of Si nanostructures on its dimensions was in good agreement with the suggested model by Suemune et al as shown in formula (7) (Alwan, A. M. 2020).

$$Eg = (Si) + (h\ 2\pi\ 2k)/ (2mr^{*}L\ 2) \quad (7)$$

Where; mr* is the reduced effective mass, k is a constant equals 2 for a pillar and 3 for SiQDs, whereas L is the dimension of nanostructures

Table 1: wavelength, intensity of PL , Eg, and e.f of hybrid SERS sensors

Sensor type	PL intensity (a.u.)	Peak emission (nm)	Energy gap(eV)	E.F
Hybrid HO-Pillars	1420	599	2.07	0.45
Based HO-Pillars	639	548	2.26	----
Hybrid SiQDs	1260	580	2.1	----
Based SiQDs	600	645	1.92	2.1

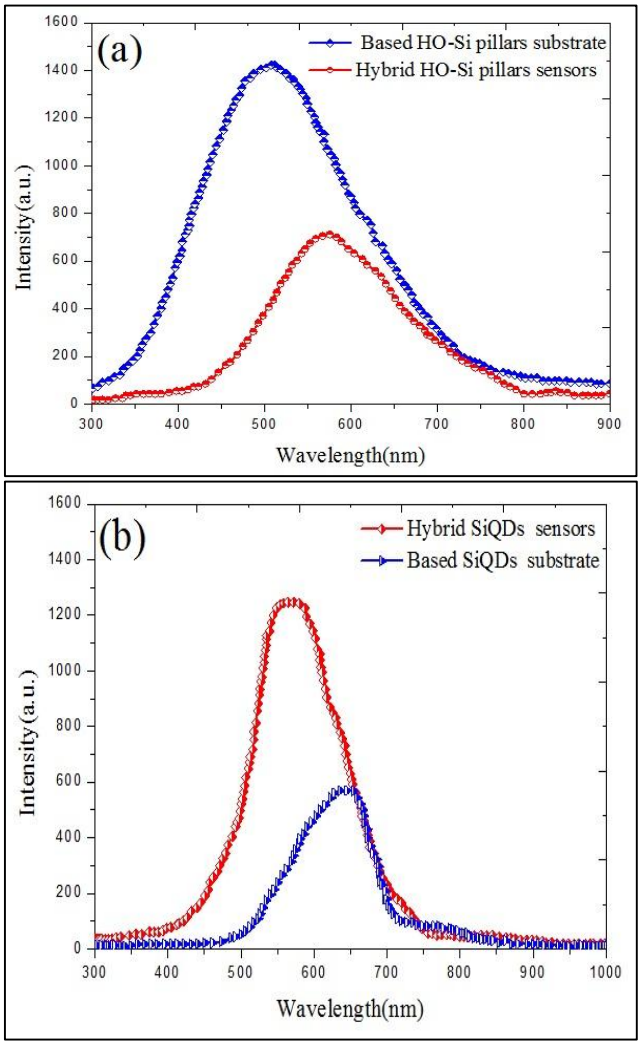

Figure 7. The PL emission of HO-Si pillars and SiQDs based- nanostructures substrate and its related hybrid SERS sensors.

3.2 Raman studies of hybrid SERS sensors

Figure 8a,b displays the Raman spectra of R6G molecules adsorbed on based HO-Si pillars and SiQDs nanostructures and its related hybrid SERS sensors of HO-Si pillars and SiQDs substrates which is excited at 532 nm . In spite of this higher concentrations of R6G molecules of about 10^{-4} M concentration ,the substrates of based HO-Si pillars and SiQDs ,show a low level of Raman signal due to the low value of Raman cross section area (Sulaiman, D. 2022). Also , this figure , display the SERS spectra of R6G dye at different concentrations ranging from 1.0×10^{-6} to1.0×10^{-12} M adsorbed on hybrid SERS sensor of Au nanoparticle / SiQDs and Au nanoparticle / HO-Si pillars . The peaks appearing at 650, 1190, 1328, 1282, and 1382 cm^{-1} are the normal Raman peaks of R6G molecules

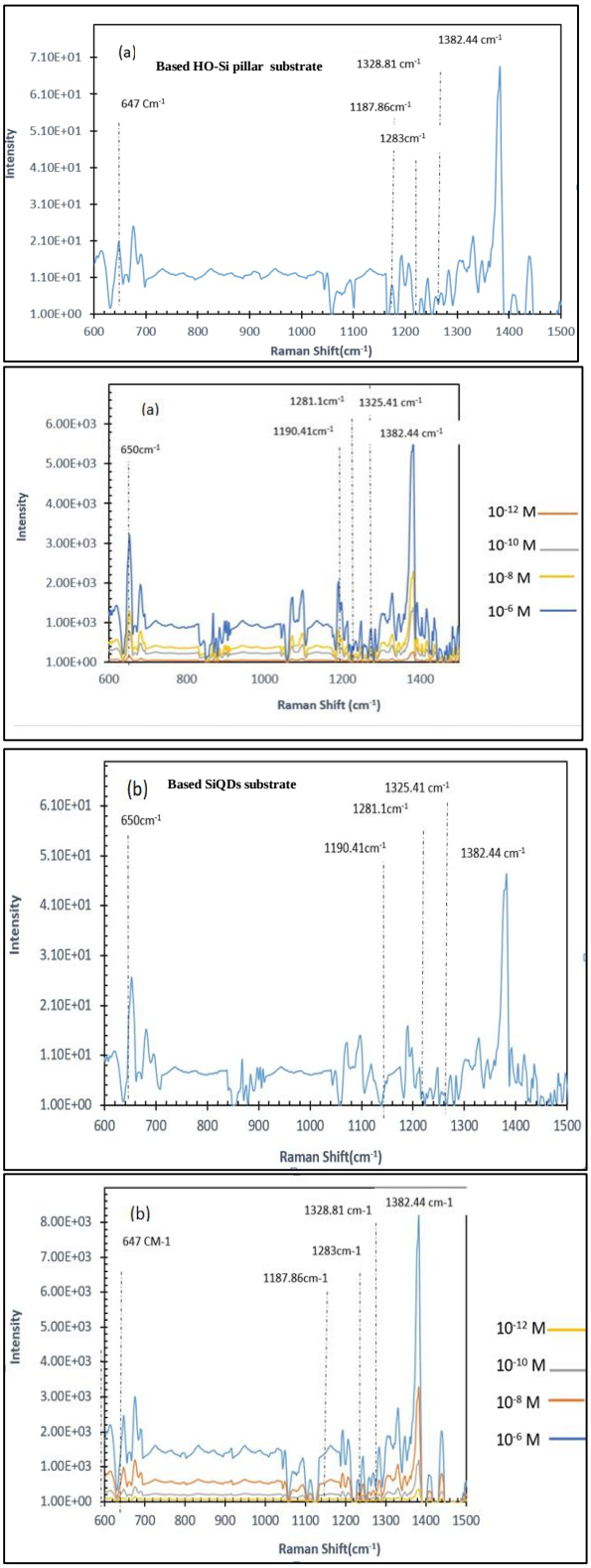

Figure 8. Raman spectra and SERS of a) HO-Si pillars and b) SiQDs.

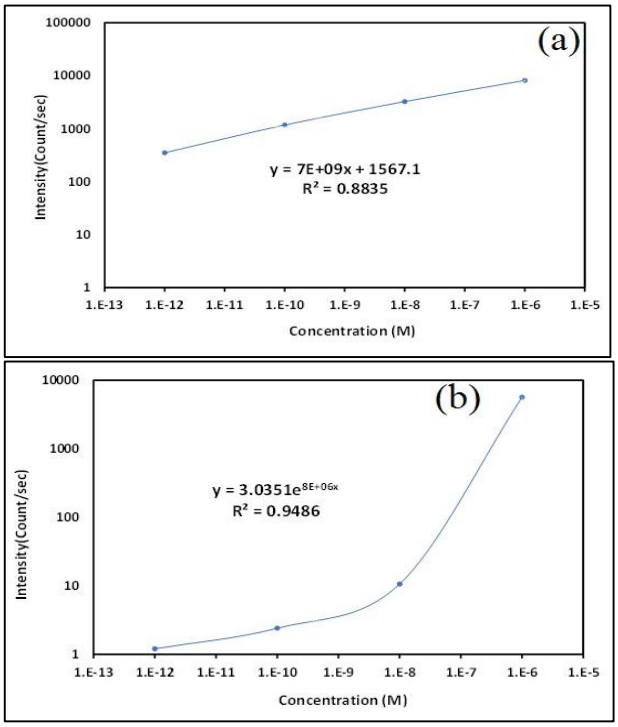

Figure 9: Relation between SERS intensity of the main Raman peak of about 1382.44 cm^{-1} and concentration for a) HO-Si pillars and b) SiQDs.

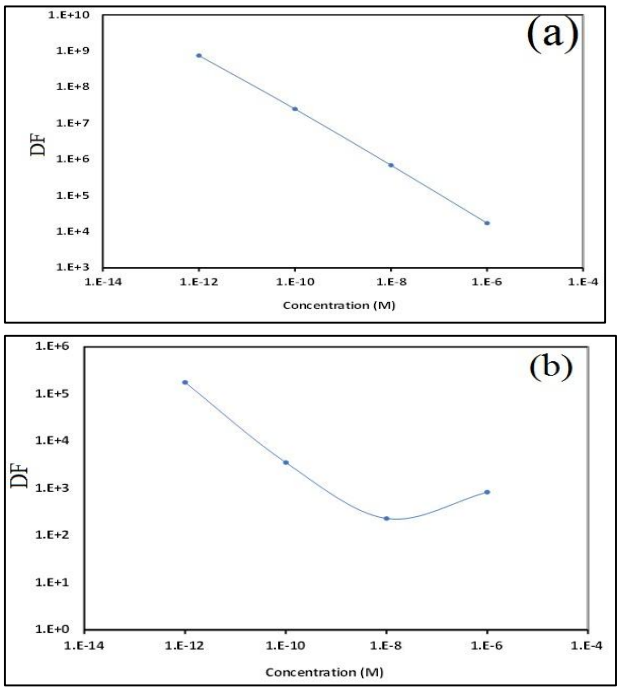

Figure 10: present the development factor of the main Raman peak of about 1382.44 cm^{-1} for a) HO-Si pillars and b) SiQDs.

To perform a quantitative analysis of the of hybrid SERS sensor of Au nanoparticle / SiQDs and Au nanoparticle / HO-Si pillars, a relationship between the characterized peak intensity 1382.44 cm^{-1} and the concentrations of R6G molecules was shown in Fig. 9a and b . The figure 9b , shows an exponential behavior of relationship of SERS signal intensity with the R6G molecules concentration from 1.0×10^{-6} to1.0×10^{-12} M as follows in equation(8)

$$\mathbf{Y=3.0351\ e^{8E+6x}\ \ with\ \ R^2=0.9486} \qquad \mathbf{(8)}$$

This type of relationship offers very high Raman output and arises due to the excitation of localized Plasmon's in Au nanoparticles when illuminated by light. The plasmonics field created by the nanoparticles strongly interacts with the adsorbed of R6G molecules, in an enhanced Raman scattering signal. The magnitude of the electromagnetic enhancement is directly proportional to the incident light intensity, which is often constant during the experiment. Therefore, the SERS signal intensity is expected to increase exponentially with R6G molecules concentration, reflecting the increased numbers of dye molecules contributing to enhance Raman scattering. For Fig. 9a, the shape of the relationship between the concentration of R6G molecules and the intensity of Raman peak of the hybrid sensor employing HO-Si pillars is linear with a low slope, which indicates inefficient response to the sensor. The linearity equation is described by the following formula (9).

$$Y=7E^{+9x}+1567.1 \quad \text{with } R^2=0.8\ 835 \qquad (9)$$

This linearity arises from the fact that the SERS enhancement process is proportional with the number of molecules participating in the scattering process. As the concentration increases, more molecules are available for interaction with the surface Plasmon's of Au nanoparticles, leading to proportional increase in the SERS signal intensity. The Raman signal intensity, can also exhibit linear behavior with the surface area (S) of the hybrid sensor. A large surface area provide more sites (hot spot regions) for the adsorption of analyte molecules and increases the probability of interaction with the enhanced electromagnetic field. Consequently, the SERS signal intensity increases linearly with the surface area. The achieved results of the hybrid SERS sensor which involves Au nanoparticle / SiQDs provide excellent opportunity for target molecules analysis. The chief cause for this distinguished behavior is due to the high density of hot spots regions among the gold nanoparticles; furthermore to the high surface of gold nanoparticles deposited on the SiQDs as well as the high surface density of SiQDs compared to the HO-Si

pillars substrate in which the surface area of the gold nanoparticles is less and its surface density is much lower. As the process of energy transfer from gold nanoparticles that are in the plasmonics state to the target molecules that are detected will increase with the increase in the density of the nanoparticles and with increase in the density of hot spots regions.

The furthermost significant factor for evaluating the activity of the hybrid SERS sensors, is the development factor (DF) of the characterized peak intensity 1382.44 cm^{-1} after integrating Au nanoparticle. The DF was computed by using equation 10 (Khalaf, A. A. 2021).

$$DF = (I_{SERS} \times C_R)/(I_R \times C_{SERS}) \quad (10)$$

Where, I_{SERS}, I_R are the signal intensities of the SERS and Raman, at the R6G concentration of C_{SERS} and C_R respectively. Figure (10 a,b) shows the DF versus the concentrations of R6G dye, adsorbed on the surface of the hybrid SERS sensor of HO-Si pillars and SiQDs, respectively. This figure, confirm that the DF increase with the decreasing of the R6G dye concentration. The highest DFs of R6G (7.46×10^8) and (1.77×10^5) at 10^{-12} M ultra-low concentration are obtained for Au nanoparticle / SiQDs hybrid sensor and for the Au nanoparticle / HO-Si pillars hybrid sensor, respectively. The R6G dye detection process is at ultra-low concentration with a higher value of DF (7.46×10^8), due to the high density of hot spots regions among the gold nanoparticles; furthermore to the high surface of gold nanoparticles deposited on the SiQDs as well as the high surface density of SiQDs compared to the HO-Si pillars.

For the synthesized hybrid sensor, based on the sensitivity relationship figure 9a,b , which signify the relation between the characterized peak intensity 1382.44 cm^{-1} and dye concentrations, the sensing limit of detection of the hybrid sensors can be calculated via using the equation (11) (Sychugov, I. 2005).

$$LOD = \frac{3S_e}{d} \quad (11)$$

Where Se is the standard deviation of characterized peak intensity Au nanoparticle / SiQDs hybrid sensor and for the Au nanoparticle / HO-Si pillars hybrid sensor, and d represents the slope of the linear portion of the sensitivity curve. The minimum achieved value of LOD is obtained from the Au nanoparticle / SiQDs hybrid sensor of about , 9*10 -14 M , whereas for Au nanoparticle / HO-Si pillars hybrid sensor the value of LOD is greater than that of SiQDs hybrid sensor by about two order of magnitude of around 1*10 -13 M.

Figure 11, displays the reproducibility of the synthesized SERS hybrid sensors. The best one is the sensor that offers the lowest difference in Raman signal. The SERS hybrid sensors, synthesized with Au nanoparticle / SiQDs, display lowest variation in Raman signal with 10 various testing positions. This excellent behavior of the hybrid sensor is connected with the homogeneity of the gold nanoparticles layer of Au nanoparticle / SiQDs. The variation of Au nanoparticle / SiQDs hybrid sensor and for the Au nanoparticle / HO-Si pillars hybrid sensor are about 4%, and 11% respectively.

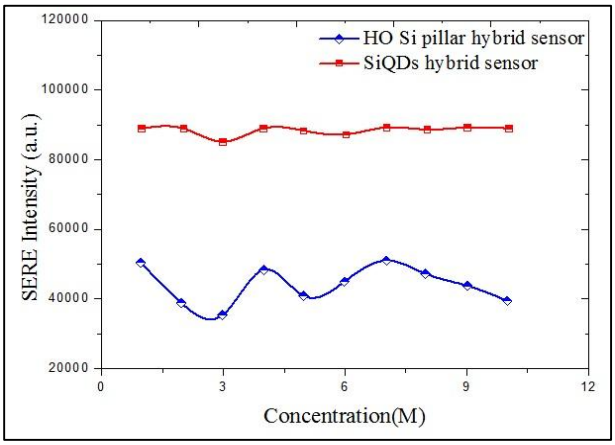

Figure 11. The reproducibility of the main Raman peak of about 1382.44 cm^{-1} for HO-Si pillars and SiQDs

2. CONCLUSIONS

In the present study, two types of hybrid SERS sensors, have been synthesized through employing integrating Au nanoparticles on HO-Si pillars and SiQDs nanostructures substrate . Uppermost Raman signal is attained for Au nanoparticle / SiQDs hybrid sensor comparing with Au nanoparticle / HO-Si pillars hybrid sensor by around two orders of magnitude was recorded. The efficiency of hybrid sensor is strongly linked with the high density of hot spots regions among the gold nanoparticles in addition to the high surface of gold nanoparticles deposited on the SiQDs as well as the high surface density of SiQDs compared to the HO-Si pillars substrate. Higher development factor, with minimum LOD and outstanding reproducibility was realized later integrating gold nanoparticles on SiQDs substrate by simple, easy –to- work and very low cost dipping technique. The results obtained from this study are of distinguished value in fabricating hybrid SERS sensors.

REFERENCES

Abed, H. R., Alwan, A. M., Yousif, A. A., & Zayer, M. Q. (2019). Efficient SnO_2/CuO/porous silicon nanocomposites structure for NH_3 gas sensing by incorporating CuO nanoparticles. *Optical and Quantum Electronics*, *51*(10), Article 333. https://doi.org/10.1007/s11082-019-2076-2

Ali, W. H., Dheyab, A. B., Alwan, M. A., & Abber, Z. S. (2020). Study the role of mud-like porous silicon morphologies on the performance of AuNPs SERS sensor for efficient detection of amoxicillin. *AIP Conference Proceedings*, *2290*, Article 050061. https://doi.org/10.1063/5.0027318

Alwan, A. M., & Ahmed, Z. S. (2014). The opto-electronic characteristics of multi-porosity silicon system. *Engineering and Technology Journal*, *32*, 811–817.

Alwan, A. M., & Ali, S. M. (2015). Gradient-porosity porous silicon (GPSi) as anti-reflection coating in solar cells applications. *Engineering and Technology Journal*, *33*(B1), 152–159.

Alwan, A. M., Dheyab, A. B., & Allaa, A. J. (2017). Study of the influence of incorporation of gold nanoparticles on the modified porous silicon sensor for petroleum gas detection. *Engineering and Technology Journal*, *35*(8A), 811–815.

Alwan, A. M., & Jabbar, A. A. (2011). Design and fabrication of nanostructures silicon photodiode. *Modern Applied Science*, *5*(1), 106–112. https://doi.org/10.5539/mas.v5n1p106

Alwan, A. M., Naseef, I. A., & Dheyab, A. B. (2018). Well controlling of plasmonic features of gold nanoparticles on macro porous silicon substrate by HF acid concentration. *Plasmonics*, *13*(6), 2037–2045. https://doi.org/10.1007/s11468-017-0667-5

Alwan, A. M., Rashid, R. B., & Dheyab, A. B. (2018). Morphological and electrical properties of gold nanoparticles/macro porous silicon for CO_2 gas. *Engineering and Technology Journal*, *59*(1A), 57–66.

Alwan, A. M., Zayer, M. Q., Jabbar, A. A., & others. (2020). Optimizing the performance of extended-gate field-effect transistor (EGFET) pH sensor by regulating the structural properties of the nanostructured porous silicon layer. *Journal of Theoretical and Applied Physics*, *14*(Suppl 1), 61–70. https://doi.org/10.1007/s40094-020-00404-7

Alwan, M. A. (2007). Calculation of energy band gap of porous silicon based on the carrier transport mechanisms. *Engineering and Technology Journal*, *25*(10), 1143–1148.

Alwan, A. M., & Abdulrazaq, O. A. (2008). Aging effect on the photosynthesized porous silicon. *International Journal of Modern Physics B*, *22*(3), 417–422. https://doi.org/10.1142/S0217979208050042

Brenner, D. J., Doll, R., Goodhead, D. T., Hall, E. J., Land, C. E., Little, J. B., Lubin, J. H., Preston, D. L., Preston, R. J., & Puskin, J. S. (2003). Cancer risks attributable to low doses of ionizing radiation: Assessing what we really know. *Proceedings of the National Academy of Sciences*, *100*(24), 13761–13766. https://doi.org/10.1073/pnas.2235592100

Canham, L. T. (1990). Silicon quantum wire array fabrication by electrochemical and chemical dissolution of wafers. *Applied Physics Letters*, *57*(10), 1046–1048. https://doi.org/10.1063/1.103561

Chalhoub, A. E., Semmar, N., Coudron, L., Gautier, G., & Boulmer-Leborgne, C. (2011). Thermal conductivity measurement of porous silicon by the pulsed-photothermal method. *Journal of Physics D: Applied Physics*, *44*(1), Article 015402. https://doi.org/10.1088/0022-3727/44/1/015402

Chang, C. C., Kuang-Hsuan, Y., Yu-Chuan, L., & Ting-Chu, H. (2012). New pathway to prepare gold nanoparticles and their applications in catalysis and surface-enhanced Raman scattering. *Colloids and Surfaces B: Biointerfaces*, *93*, 169–173. https://doi.org/10.1016/j.colsurfb.2011.12.031

Cheng, X. Y., Hinde, E., Owen, D. M., Lowe, S. B., Reece, P. J., Gaus, K., & Gooding, J. J. (2015). Enhancing quantum dots for bioimaging using advanced surface chemistry and advanced optical microscopy: Application to silicon quantum dots (SiQDs). *Advanced Materials*, *27*(36), 6144–6150. https://doi.org/10.1002/adma.201502281

Dheyab, A. B., Alwan, A. M., & Zayer, M. Q. (2019). Optimizing of gold nanoparticles on porous silicon morphologies for a sensitive carbon monoxide gas sensor device. *Plasmonics*, *14*(2), 501–509. https://doi.org/10.1007/s11468-018-0803-1

Ershov, I. A., Iskhakova, L. D., Krasovskii, V. I., Milovich, F. O., Rasmagin, S. I., & Pustovoi, V. I. (2020). Synthesis of silicon-carbide nanoparticles by the laser pyrolysis of a mixture of monosilane and acetylene. *Semiconductors*, *54*(11), 1467–1471. https://doi.org/10.1134/S1063782620110033

Giorgis, F., Descrovi, E., Chiodoni, A., Froner, E., Scarpa, M., Venturello, A., & Geobaldo, F. (2008). Porous silicon as efficient surface enhanced Raman scattering (SERS) substrate. *Applied Surface Science*, *254*(22), 7494–7497. https://doi.org/10.1016/j.apsusc.2008.05.323

Hamoudi, W. K., Alwan, M. A., & Sulaiman, D. (2020). Controllable formation of plasmonic gold nanoparticles by pulsed laser–induced etching.

Optical and Quantum Electronics, *52*, Article 351. https://doi.org/10.1007/s11082-020-02466-w

He, Y., Xiao, S., Dong, T., & Nie, P. (2019). Gold nanoparticles with different particle sizes for the quantitative determination of chlorpyrifos residues in soil by SERS. *International Journal of Molecular Sciences*, *20*(11), 2817. https://doi.org/10.3390/ijms20112817

Hou, X., Zhang, X., Chen, S., Fang, Y., Li, N., Zhai, X., & Liu, Y. (2011). Size-controlled synthesis of Au nanoparticles and nanowires and their application as SERS substrates. *Colloids and Surfaces A: Physicochemical and Engineering Aspects*, *384*(1–3), 345–351. https://doi.org/10.1016/j.colsurfa.2011.04.018

Jabbar, A. A., Alwan, M. A., Zayer, M. Q., & Azhar, J. (2020). Efficient single cell monitoring of pathogenic bacteria using bimetallic nanostructures embedded in gradient porous silicon. *Materials Chemistry and Physics*, *241*, Article 122359. https://doi.org/10.1016/j.matchemphys.2019.122359

Jubair, D. S., Alwan, M. A., & Hamoudi, W. K. (2021). Sensing performance of mono and bimetallic nano photonics surface enhanced Raman scattering (SERS) devices. *Engineering and Technology Journal*, *39*(7), 1174–1184.

Khalaf, A. A., Alwan, A. M., Attallah, A. H., & Dheyab, A. B. (2021). Influence of magnetic field on the characteristics of n-type porous silicon prepared by photo-electro-chemical etching process. *Journal of Physics: Conference Series*, *1963*, Article 012015. https://doi.org/10.1088/1742-6596/1963/1/012015

Ko, F. H., Tai, M. R., Liu, F. K., & Chang, Y. C. (2015). Au–Ag core–shell nanoparticles with controllable shell thicknesses for the detection of adenosine by surface enhanced Raman scattering. *Sensors and Actuators B: Chemical*, *211*, 283–289. https://doi.org/10.1016/j.snb.2015.01.052

Kumar, V., Saxena, K., & Shukla, A. K. (2013). Size-dependent photoluminescence in silicon nanostructures: Quantum confinement effect. *Micro & Nano Letters*, *8*(6), 311–314. https://doi.org/10.1049/mnl.2013.0086

Liu, L. R., Zhu, G. B., Zeng, W., Yi, Y. H., Lv, B. H., Qian, J. J., & Zhang, D. P. (2019). Silicon quantum dot-coated onto gold nanoparticles as an optical probe for colorimetric and fluorometric determination of cysteine. *Microchimica Acta*, *186*(2), Article 98. https://doi.org/10.1007/s00604-018-3162-1

Liu, Y. N., Wang, Q. Z., Guo, S. W., Jia, P., Shui, Y. H., Yao, S. Y., Huang, C., Zhang, M., & Wang, L. (2018). Highly selective and sensitive fluorescence detection of hydroquinone using novel silicon quantum dots. *Sensors and Actuators B: Chemical*, *275*, 415–421. https://doi.org/10.1016/j.snb.2018.08.066

Naseef, I. A., & Alwan, A. M. (2017). Optimization of photoluminescence properties of porous silicon by adding gold nanoparticles. *Iraqi Journal of Science*, *58*(1A), 53–62.

Naseef, I. A., Dheyab, A. B., Wali, L. A., & Alwan, A. M. (2019). Perfect incorporation of AuNPs on the p-n+ porous silicon for highly-efficient solar cells. *Optik*, *198*, Article 163317. https://doi.org/10.1016/j.ijleo.2019.163317

Pohl, U. W. (2018). Low-dimensional semiconductors. In *Springer Handbook of Materials Data* (pp. 1081–1104). Springer. https://doi.org/10.1007/978-3-319-38925-7_37

Rashid, R. B., Alwan, M. A., & Mohammed, M. S. (2022). Improved difenoconazole pesticide detection limit via double-sided porous silicon layers' electrical sensor. *Materials Chemistry and Physics*, *287*, Article 126286. https://doi.org/10.1016/j.matchemphys.2022.126286

Sulaiman, D., Alwan, A. M., & Hamoudi, W. K. (2022). Pesticide detection optimization of plasmonic gold nanoparticles/silicon nano-columns structures by controlling the coupling lasers power density. *Gold Bulletin*, *55*, 19–30. https://doi.org/10.1007/s13404-022-00323-x

Sychugov, I., Juhasz, R., Linnros, J., & Valenta, J. (2005). Luminescence blinking of a Si quantum dot in a SiO_2 shell. *Physical Review B*, *71*(11), Article 115331. https://doi.org/10.1103/PhysRevB.71.115331

Wali, L. A., Dheyab, A. B., & Alwan, A. M. (2023). Study the influence of shell thickness in bimetallic Ag core & Au shell configurations integrated in bare Si PN junction solar cells. *Materials Science in Semiconductor Processing*, *288*, Article 116210. https://doi.org/10.1016/j.mseb.2023.116210

Wali, L. A., Hasan, K. K., & Alwan, A. M. (2020). An investigation of efficient detection of ultra-low concentration of penicillins in milk using AuNPs/PSi hybrid structure. *Plasmonics*, *15*, 1487–1495. https://doi.org/10.1007/s11468-020-01220-0

Wail, H. A., Dheyab, A. B., & Alwan, A. M. (2018). Optimization and synthesis of gold nanoparticles on N-type porous silicon substrates as highly-gas sensitive. *International Journal of Mechanical Engineering and Technology*, *9*(10), 1393–1401.

Wang, X., Zhang, E., Shi, H., Tao, Y., Ren, X., & Zi, J. (2022). Semiconductor-based surface enhanced Raman scattering (SERS): From active materials to performance improvement. *Analyst*, *147*(7), 1257–1272. https://doi.org/10.1039/D1AN02082D

Xu, S. H., Xiong, Z. H., Gu, L. L., Liu, Y., Ding, X. M., Zi, J., & Hou, X. Y. (2003a). Preparation of one-dimensional porous silicon photonic quantum-well structures. *Applied Physics A*, *76*(4), 589–592. https://doi.org/10.1007/s00339-002-1935-2

Xu, S. H., Xiong, Z. H., Gu, L. L., Liu, Y., Ding, X. M., Zi, J., & Hou, X. Y. (2003b). Photon confinement in one-dimensional photonic quantum-well structures of nanoporous silicon. *Solid State Communications*, *126*(2), 125–128. https://doi.org/10.1016/S0038-1098(03)00270-1

Zhang, Y., Gu, C., Schwartzberg, A. M., & Zhang, J. Z. (2005). Surface-enhanced Raman scattering sensor based on D-shaped fiber. *Applied Physics Letters*, *87*(12), Article 123105. https://doi.org/10.1063/1.2048816